

The Evolution of Luminous Matter in the Universe

Piero Madau

Space Telescope Science Institute, 3700 San Martin Drive, Baltimore, MD 21218

Abstract. I review a technique for interpreting faint galaxy data which traces the evolution with cosmic time of the galaxy luminosity density, as determined from several deep spectroscopic samples and the *Hubble Deep Field* imaging survey. The method relies on the rest-frame UV and near-IR continua of galaxies as indicators, for a given initial mass function (IMF) and dust content, of their instantaneous star formation rate (SFR) and total stellar mass, and offers the prospect of addressing in a coherent framework an important set of subjects: cosmic star formation history, dust in primeval galaxies, shape of the IMF, stellar mass-to-light ratios of present-day galaxies, extragalactic background light, Type II supernovae and heavy element enrichment history of the universe. The global spectrophotometric properties of field galaxies are well fit by a simple stellar evolution model, defined by a time-dependent SFR per unit comoving volume, a universal IMF which is relatively rich in massive stars, and a modest amount of dust reddening. The model is able to account for the entire background light recorded in the galaxy counts down to the very faint magnitude levels probed by the HDF, and produces visible mass-to-light ratios at the present epoch which are consistent with the values observed in nearby galaxies of various morphological types. The bulk ($\gtrsim 60\%$) of the stars present today formed relatively recently ($z \lesssim 1.5$), consistently with the expectations from a broad class of hierarchical clustering cosmologies, and in good agreement with the low level of metal enrichment observed at high redshifts in the damped Lyman- α systems. Throughout this review I emphasize how the poorly constrained amount of starlight that was absorbed by dust and reradiated in the far-IR at early epochs represents one of the biggest uncertainties in our understanding of the evolution of luminous matter in the universe. A “monolithic collapse” model, where half of the present-day stars formed at $z > 2.5$ and were enshrouded by dust, can be made consistent with the global history of light, but overpredicts the metal mass density at high redshifts as sampled by QSO absorbers.

1. Introduction

As the best view to date of the optical sky at faint flux levels, the *Hubble Deep Field* (HDF) has offered to many astronomers the opportunity to study the galaxy population in unprecedented details. In particular, the deep HDF images have rapidly become a key testing ground for the two competing scenarios that have been widely used in the past few years to interpret the observed properties of galaxies. In what may be called the “traditional” scheme, one starts from the local measurements of the distribution of galaxies as a function of luminosity and Hubble type and models their photometric evolution assuming a well defined collapse epoch, pure-luminosity evolution thereafter, and a set of parameterized star formation histories (Tinsley 1980; Bruzual & Kron 1980; Koo 1985; Pozzetti, Bruzual, & Zamorani 1996). These, together with an initial mass function (IMF) and a

world model, are then adjusted to match the observed number counts, colors, and redshift distributions. Beyond its intrinsic simplicity, the main advantage of this kind of approach is that it can be made consistent with the classical view that ellipticals and spiral galaxy bulges formed early in a single burst of duration 1 Gyr or less (e.g., Bower et al. 1992; Ortolani et al. 1995). Because in this “monolithic” collapse scenario for spheroids much of the action happens at high- z , however, these models predict, in the absence of a significant amount of dust obscuration, far more Lyman-break “blue dropouts” than are seen in the HDF (Pozzetti et al. 1997; Ferguson & Babul 1997). Moreover, they cannot reproduce the rapid evolution – largely driven by late-type galaxies – of the optical luminosity density with lookback time observed by Lilly et al. (1996) and Ellis et al. (1996).

A more physically motivated way to interpret the observations is to construct semianalytic hierarchical models of galaxy formation and evolution (White & Frenk 1991; Kauffmann, White, & Guiderdoni 1993; Cole et al. 1994; Baugh et al. 1997). Here, one starts from a power spectrum of primordial density fluctuations, follows the growth of dark matter halos by accretion and mergers, and adopts various prescriptions for gas cooling, star formation, feedback from supernovae and stellar winds, and dynamical friction. These are tuned to match the statistical properties of both nearby and distant galaxies. In this scenario, there is no period when bulges and ellipticals form rapidly as single units and are very bright: rather, small objects form first, eventually settling into disks, and merge continually over a range of redshifts to make ellipticals (see reviews by G. Kauffmann and S. White in these proceedings). While reasonably successful in recovering the counts, colors, and redshift distributions of faint galaxies, a generic difficulty of such models is the inability to simultaneously reproduce the observed local luminosity density and the zero-point of the Tully-Fisher relation (White & Frenk 1991; Cole et al. 1994).

In this talk I will describe an alternative method, which focuses on the emission properties of the galaxy population *as a whole*. It traces the cosmic evolution with redshift of the galaxy luminosity density – as determined from several deep spectroscopic samples and the HDF imaging survey – and offers the prospect of an empirical determination of the global star formation history of the universe and initial mass function of stars independently, e.g., of the merging histories and complex evolutionary phases of individual galaxies. The technique relies on two basic properties of stellar populations: a) the UV-continuum emission in all but the oldest galaxies is dominated by short-lived massive stars, and is therefore a direct measure, for a given IMF and dust content, of the instantaneous star formation rate (SFR); and b) the rest-frame near-IR light is dominated by near-solar mass evolved stars that make up the bulk of a galaxy’s visible mass, and can then be used as a tracer of the integrated stellar mass density. By modeling the “emission history” of the universe at ultraviolet, optical, and near-infrared wavelengths from the present epoch to $z \approx 4$, I will try to shed some light on what I believe are key questions in structure formation and evolution studies, and provide a first glimpse to the history of the conversion of neutral gas into stars within galaxies.

The initial applications of this novel technique have been presented by Lilly et al. (1996), Madau et al. (1996, hereafter M96), and Madau, Pozzetti, & Dickinson (1997). A complementary effort – which starts instead from the analysis of the evolving gas content and metallicity of the universe – can be found in Fall, Charlot, and Pei (1996). A flat cosmology with $q_0 = 0.5$ and $H_0 = 50 h_{50} \text{ km s}^{-1} \text{ Mpc}^{-1}$ will be adopted in this review.

2. Indicators of Past and Present Star Formation Activity

Stellar population synthesis has become a standard technique to study the spectrophotometric properties of galaxies. In the following, I shall make extensive use of the latest

version of Bruzual & Charlot (1993) isochrone synthesis code, optimized with an updated library of stellar spectra (Bruzual & Charlot 1997), to predict the time change of the spectral energy distribution of a stellar population. I will consider here two possibilities for the IMF, a Salpeter (1955) function and a Scalo (1986) IMF, which is flatter for low-mass stars and significantly less rich in massive stars than Salpeter. In all models the metallicity is fixed to solar values and the IMF is truncated at 0.1 and 125 M_{\odot} .

2.1. Birthrate–Ultraviolet Relation

The UV continuum emission from a galaxy with significant ongoing star formation is entirely dominated by late-O/early-B stars on the main sequence. As these have masses $\gtrsim 10 M_{\odot}$ and lifetimes $t_{MS} \lesssim 2 \times 10^7$ yr, the measured luminosity becomes proportional to the stellar birthrate and independent of the galaxy history for $t \gg t_{MS}$. This is depicted in Figure 1, where the power radiated at 1500 Å and 2800 Å is plotted against the instantaneous SFR for a model stellar population with different star formation laws, $\text{SFR} \propto \exp(-t/\tau)$, where τ is the duration of the burst. After an initial transient phase where the UV flux rises rapidly and the turnoff mass drops below $10 M_{\odot}$, a steady state is reached

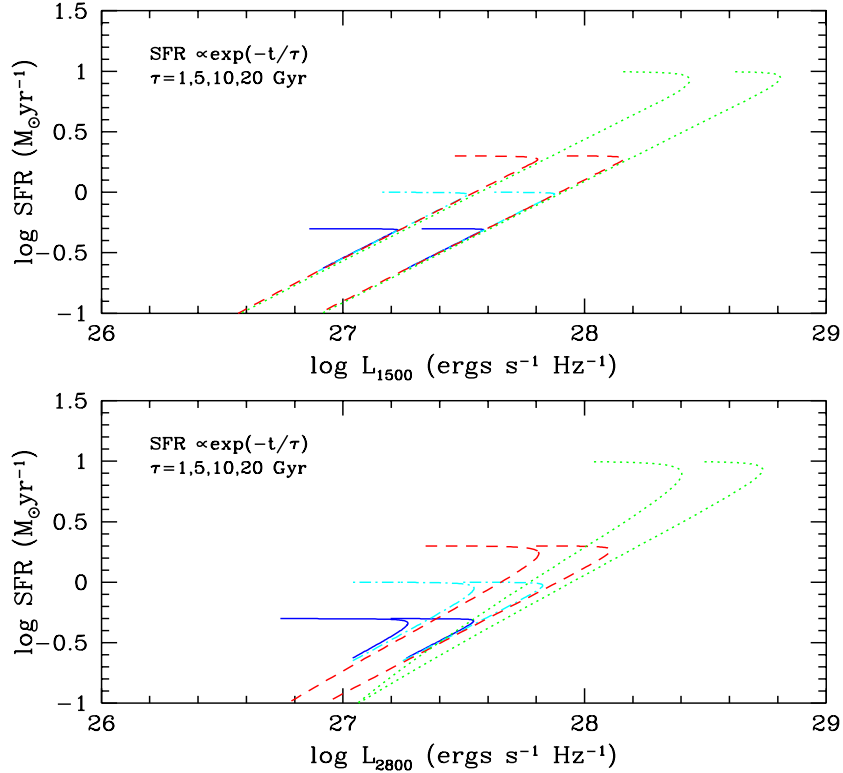


Figure 1. SFR-UV relation for models with various exponentially declining star formation rates at ages between 0.01 and 15 Gyr. *Solid lines*: $\tau = 20$ Gyr. *Dot-dashed lines*: $\tau = 10$ Gyr. *Dashed lines*: $\tau = 5$ Gyr. *Dotted lines*: $\tau = 1$ Gyr. The set of curves on the left-hand side of the plot assume a Scalo IMF, the ones on the right-hand side a Salpeter function.

where one can write

$$L_{UV} = \text{const} \times \frac{\text{SFR}}{\text{M}_{\odot} \text{ yr}^{-1}} \text{ ergs s}^{-1} \text{ Hz}^{-1}, \quad (1)$$

with $\text{const} = (3.5 \times 10^{27}, 5.0 \times 10^{27})$ at $(1500 \text{ \AA}, 2800 \text{ \AA})$ for a Scalo IMF, and $\text{const} = 8.0 \times 10^{27}$ in the same wavelength range for a Salpeter IMF, quite insensitive to the details of the past star formation history. Note how, for burst durations $\lesssim 1 \text{ Gyr}$ and a Scalo IMF, the luminosity at 2800 \AA becomes a poor SFR indicator after a few e -folding times, when the contribution of intermediate-mass stars becomes significant. After averaging over the whole galaxy population, however, we will find that the (unreddened) UV continuum is always a good tracer of the instantaneous rate of conversion of cold gas into stars.

2.2. Birthrate– $\text{H}\alpha$ Relation

In the optical wavelength range, the $\text{H}\alpha$ ($\lambda 6563$) luminosity from a galaxy is another probe of its current star formation activity (Kennicutt 1983), as, for ionization bounded H II regions, the integrated line emission scales directly with the Lyman-continuum flux of the embedded OB stars. Assuming case-B recombination theory and a Salpeter function, the $\text{H}\alpha$ luminosity can be related to the local SFR according to

$$L_{\text{H}\alpha} = 1.5 \times 10^{41} \left(\frac{\text{SFR}}{\text{M}_{\odot} \text{ yr}^{-1}} \right) \text{ ergs s}^{-1}. \quad (2)$$

The coefficient for a Scalo IMF is approximately four times smaller. Note that, shortward of the Lyman edge, the differences in the predicted ionizing radiation from model atmospheres of hot stars can be quite large (Charlot 1996a), and must be taken into account when interpreting the results of surveys for $\text{H}\alpha$ -emitting galaxies (Gallego et al. 1995).

2.3. Supernova Frequency

The frequency of supernovae (SNe) is also intimately related, for a given IMF, to the stellar birthrate. This is true, in particular, for “core-collapse supernovae”, SN II and SN Ib/c, which have massive, short-lived ($t_{\text{MS}} \lesssim 2 \times 10^7 \text{ yr}$) progenitors. It might also be approximately true for Type Ia SNe – believed to result from the thermonuclear disruption of accreting CO white dwarfs in binary systems (for a recent review see Ruiz-Lapuente, Canal, & Burkert 1997) – if the favourite route follows a fast evolutionary track, and the deflagration occurs within few Gyr of (binary) stellar birth. Since the Hubble time is equal to 3 Gyr at $z = 1.7$, it would then be possible to neglect the delay between stellar birth and the SN Ia it eventually yields at all epochs $z \ll 1.7$ (but see Yungelson & Livio 1997).

For a Salpeter IMF and a lower mass cutoff for the progenitor star of 10 M_{\odot} , the core-collapse supernova rate (SNR) can be related to the stellar birthrate according to

$$\text{SNR} = 0.0055 \times \left(\frac{\text{SFR}}{\text{M}_{\odot} \text{ yr}^{-1}} \right) \text{ yr}^{-1}. \quad (3)$$

The coefficient for a Scalo IMF is 2.6 times smaller. I will show later how SNe may provide an independent test of the global star formation history of the universe at low redshifts.

2.4. Mass–Infrared Relation

If we assume a time-independent IMF, we can use the results of stellar population synthesis modeling, together with the observed UV emissivity, to infer the evolution of the star formation activity in the universe (M96). The biggest uncertainty in this procedure is due to dust reddening, as newly formed stars which are completely hidden by dust would not

contribute to the UV luminosity. The effect is potentially more serious at high redshifts, as for a fixed observer-frame bandpass, one is looking further in the ultraviolet with increasing lookback time. For example, SMC-type foreground dust with $E(B - V) \gtrsim 0.1$ would produce an extinction at 1500 \AA greater than 1.3 magnitudes. On the other hand, it should be possible to test the hypothesis that star formation regions remain largely unobscured by dust throughout much of galaxy evolution by looking at the near-infrared light density. This will be affected by dust only in the most extreme, rare cases, as it takes an $E(B - V) > 4$ mag to produce an optical depth of unity at $2.2 \text{ }\mu\text{m}$.

Although different types of stars – such as supergiants, AGB, and red giants – dominate the K -band emission at different ages in an evolving stellar population, the mass-to-infrared light ratio is relatively insensitive to the star formation history (Charlot 1996b). Figure 2 shows M/L_K (in solar units) as a function of age for models with various exponentially declining SFR compared to the values observed in nearby galaxies of early to late morphological types. As the stellar population ages, the mass-to-infrared light ratio remains very close to unity, independent of the galaxy color and Hubble type. We can use

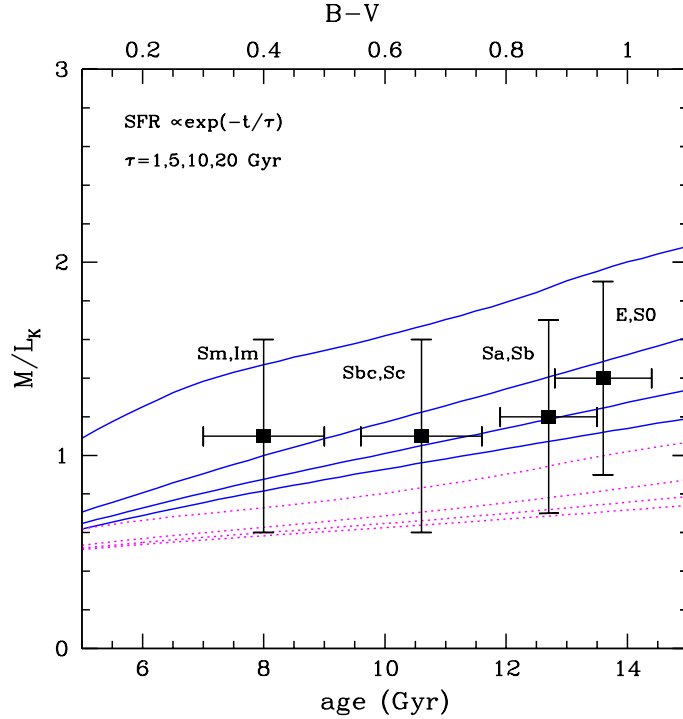


Figure 2. Total (processed gas+stars) mass-to- K band light ratio versus age for models with various exponentially declining star formation rates. *Solid lines*: Salpeter IMF. *Dotted lines*: Scalo IMF. From top to bottom, each set of curves depict the values for $\tau = 1, 5, 10$, and 20 Gyr , respectively. The data points show the luminous mass-to-infrared light ratio versus $B - V$ color (top axis) observed in nearby galaxies of various morphological types (see Charlot 1996b). The observations refer to the mass within the galaxy Holmberg radius, where the contribution by the dark matter halo is expected to be small.

this interesting property to estimate the visible mass in galaxies from the local K -band luminosity density, $\log \rho_K(0) = 27.05 \pm 0.1 h_{50} \text{ ergs s}^{-1} \text{ Hz}^{-1} \text{ Mpc}^{-3}$ (Gardner et al. 1997). The observed range $0.6 h_{50} \lesssim M/L_K \lesssim 1.9 h_{50}$ translates into a mass density of stars+gas at the present day of

$$2 \times 10^8 \lesssim \rho_{s+g}(0) \lesssim 6 \times 10^8 h_{50}^2 \text{ M}_\odot \text{ Mpc}^{-3} \quad (4)$$

($0.003 \lesssim \Omega_{s+g} \lesssim 0.009$). I will show later how the observed integrated UV emission, with the addition of some modest amount of reddening, may account for the bulk of the baryons traced by the K -band light, and how initial mass functions with relatively few high-mass stars (such as the Scalo IMF), or models with a large amount of dust extinction at all epochs will tend to overproduce the near-infrared emissivity.

3. Galaxy Emissivity as a Function of Redshift

The integrated light radiated per unit volume from the entire galaxy population is an average over cosmic time of the stochastic, possibly short-lived star formation episodes of individual galaxies, and should follow a relatively simple dependence on redshift. In the UV – where it is proportional to the global SFR – its evolution should provide information on the mechanisms which may prevent the gas within virialized dark matter halos from radiatively cooling and turning into stars at early times, or on the epoch when galaxies exhausted their reservoirs of cold gas. From a comparison between different wavebands it should be possible to set constraints on the average IMF and dust content of galaxies.

The observed continuum emissivity, $\rho_\nu(z)$, from the present epoch to $z \approx 4$ is shown in Figure 3 in six broad passbands centered around 0.15, 0.2, 0.28, 0.44, 1.0, and 2.2 μm . The data are taken from the K -selected redshift survey of Gardner et al. (1997) and Cowie et al. (1996), the I -selected CFRS (Lilly et al. 1996) and B -selected Autofib (Ellis et al. 1996) samples, a redshift survey of galaxies imaged in the rest-frame ultraviolet at 2000 \AA with the FOCA balloon-borne camera (Treyer et al. 1997), the photometric redshift catalog for the HDF of Connolly et al. (1997) – which take advantage of deep infrared observations by Dickinson et al. (1997) –, and the color-selected UV and blue “dropouts” of M96 (see also Madau 1997). They have all (except for the Treyer et al. value) been corrected for incompleteness by integrating over the best-fit Schechter function in each redshift bin,

$$\rho_\nu(z) = \int L_\nu \phi(L_\nu, z) dL_\nu = \Gamma(2 + \alpha) \phi_* L_*. \quad (5)$$

As it is not possible to reliably determine the faint end slope of the luminosity function from the Connolly et al. (1997) and M96 data sets, a value of $\alpha = -1.3$ has been assumed at each redshift interval for comparison with the CFRS sample (Lilly et al. 1995). The error bars are typically less than 0.2 in the log, and reflect the uncertainties present in these corrections and, in the HDF $z > 2$ sample, in the volume normalization and color-selection region.

Despite the obvious caveats due to the likely incompleteness in the data sets, different selection criteria, and existence of systematic uncertainties in the photometric redshift technique, the spectroscopic, photometric, and Lyman-break galaxy samples appear to provide a remarkably consistent picture of the emission history of field galaxies.¹ This points to a rapid drop in the volume-averaged SFR in the last 8–10 Gyr, and to a redshift range where the bulk of the stellar population was actually assembled: $1 \lesssim z \lesssim 2$.

¹While there is no evidence for a gross mismatch at the $z \approx 2$ transition between the photometric redshift sample of Connolly et al. (1997) and the M96 UV dropout sample, one should note that only one spectroscopic confirmation has been obtained so far at $z \approx 4$ (Dickinson 1997).

4. Population Synthesis

It is interesting to see now whether a simple stellar evolution model, defined by a time-dependent SFR per unit volume and a universal IMF, may reproduce the global UV, optical, and near-IR photometric properties of galaxies. In a stellar system with arbitrary star formation rate, the luminosity density at time t is given by the convolution integral

$$\rho_\nu(t) = \int_0^t L_\nu(\tau) \times \text{SFR}(t - \tau) d\tau, \quad (6)$$

where $L_\nu(\tau)$ is the specific luminosity radiated per unit initial mass by a generation of stars with age τ . After relating the observed UV continuum emissivity to a SFR density, one can then use, e.g., Bruzual-Charlot's synthesis code to predict the time evolution of the spectrophotometric properties of a stellar population in a comoving volume large enough to

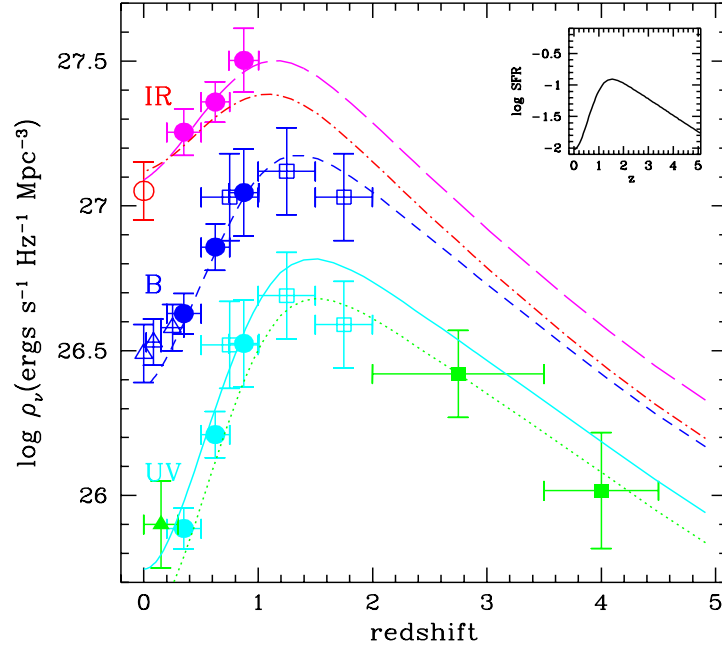


Figure 3. Evolution of the comoving luminosity density at rest-frame wavelengths of 0.15 (*dotted line*), 0.28 (*solid line*), 0.44 (*short-dashed line*), 1.0 (*long-dashed line*), and 2.2 (*dot-dashed line*) μm . The data points with error bars are taken from Lilly et al. (1996) (*filled dots*), Connolly et al. (1997) (*empty squares*), Madau et al. (1996) and Madau (1997) (*filled squares*), Ellis et al. (1996) (*empty triangles*), Treyer et al. (1997) (*filled triangle*), and Gardner et al. (1997) (*empty dot*). The inset in the upper-right corner of the plot shows the SFR density ($\text{M}_\odot \text{ yr}^{-1} \text{ Mpc}^{-3}$) versus redshift which was used as input to the population synthesis code. The model assumes a Salpeter IMF, SMC-type dust in a foreground screen, and a universal $E(B - V) = 0.1$.

be representative of the universe as a whole. In doing so, we will bypass all the ambiguities associated with the study of morphologically distinct samples, but, at the same time, we will not be able to specifically address the evolution of particular subclasses of objects, like the oldest ellipticals, whose star formation histories may have differed significantly from the global average. It is fair at this stage to point out two other significant limitations of this approach: a) It focuses on the emission properties of “normal”, optically-selected field galaxies which are only moderately affected by dust – a typical spiral emits 30% of its energy in the far-infrared region (Saunders et al. 1990). Starlight which is completely blocked from view even in the near-IR by a large optical depth in dust will not be recorded by this technique, and the associated baryonic mass and metals missed from our census. The contribution of infrared-selected dusty starbursts to the present-day total stellar mass density cannot be very large, however, for otherwise the current limits to the energy density of the mid- and far-infrared background would be violated (Puget et al. 1996; Kashlinsky, Mather, & Odenwald 1996; Fall et al. 1996; Guiderdoni et al. 1997). Locally, infrared luminous galaxies are known to produce only a small fraction of the IR luminosity of the universe (Soifer & Neugebauer 1991); and b) It does not include the effects of cosmic chemical evolution on the predicted galaxy colors. All the population synthesis models assume solar metallicity, and thus will generate colors that are slightly too red for objects with low metallicity, e.g. truly primeval galaxies.

4.1. A Fiducial Model: Salpeter IMF

Figure 3 shows the model predictions for the evolution of ρ_ν at rest-frame ultraviolet to near-infrared frequencies for a Salpeter IMF. In the absence of dust reddening, this relatively flat IMF generates spectra that are slightly too blue to reproduce the observed mean (luminosity-weighted over the entire population) galaxy colors. The effect of dust attenuation can be included by multiplying equation (6) by p_{esc} , a redshift-independent term equal to the fraction of emitted photons which are not absorbed by dust. For purposes of illustration, I will assume a foreground screen model, $p_{\text{esc}} = \exp(-\tau_\nu)$, and SMC-type dust.² This should only be regarded as a crude approximation, since hot stars can be heavily embedded in dust within star-forming regions, there will be variety of extinction laws, and the dust content of galaxies will evolve with redshift. While the existing data are too sparse to warrant a more elaborate analysis, this simple prescription will highlight the main features and assumptions of the model. The shape of the predicted and observed $\rho_\nu(z)$ relations is then found to agree better to within the uncertainties if a modest amount of dust extinction, $E(B - V) = 0.1$, is included. In this case, the observed UV luminosities must be corrected upwards by a factor of 1.4 at 2800 Å and 2.1 at 1500 Å.

As expected, while the ultraviolet emissivity traces remarkably well the rise, peak, and sharp drop in the instantaneous star formation rate (the smooth function shown in the inset on the upper-right corner of the figure), an increasingly large component of the longer wavelengths light reflects the past star formation history. The peak in the luminosity density at 1.0 and 2.2 μm occurs then at later epochs, while the decline from $z \approx 1$ to $z = 0$ is more gentle than observed at shorter wavelengths. In the instantaneous recycling approximation (Tinsley 1980), the total stellar mass density produced at time t is

$$\rho_s(t) = (1 - R) \int_0^t \text{SFR}(t) dt, \quad (7)$$

²Since what is relevant here is the absorption opacity, I have multiplied the extinction optical depth by a factor of 0.6, as the albedo of dust grains is known to approach asymptotically 0.4–0.5 at ultraviolet wavelengths (see, e.g., Pei 1992).

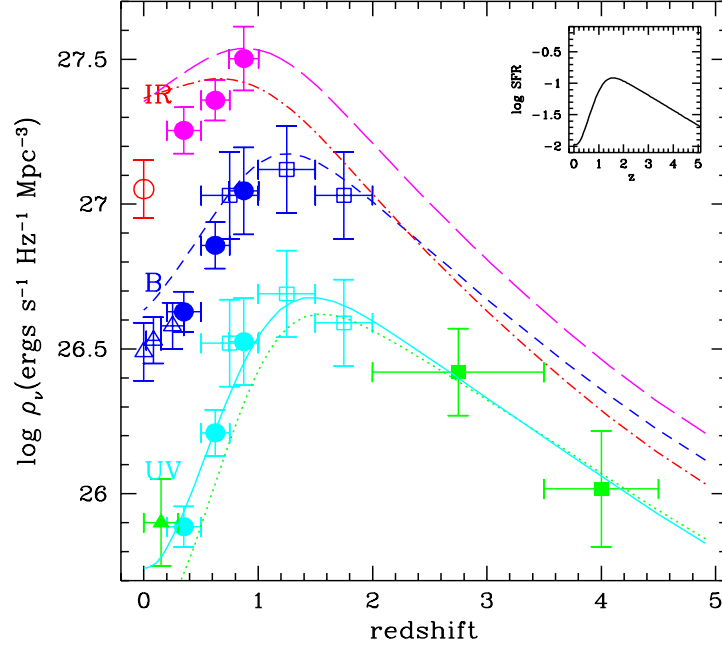


Figure 4. Same as in Figure 3, but assuming a Scalo IMF and no dust extinction. This model overproduces the local K -band emissivity by a factor of 2.

where R is the mass fraction of a generation of stars that is returned to the interstellar medium, $R \approx 0.3$ for a Salpeter IMF (R is closer to 0.2 for a Scalo function). The total stellar mass density at $z = 0$ is then $\rho_s(0) = 3.7 \times 10^8 M_\odot \text{ Mpc}^{-3}$, with a fraction close to 65% being produced at $z > 1$, and only 20% at $z > 2$. In the assumed cosmology, about half of the stars observed today are more than 9 Gyr old, and only 20% are younger than 5 Gyr.

4.2. A Case with a Scalo IMF

Figure 4 shows the model predictions for a Scalo IMF. The fit to the data is now much poorer, since this IMF generates spectra that are too red to reproduce the observed mean galaxy colors, as first noted by Lilly et al. (1996). Because of the relatively large number of solar mass stars formed, it produces too much long-wavelength light by the present epoch. The addition of dust reddening would obviously make the fit even worse. The total stellar mass density produced is similar to the Salpeter IMF case.

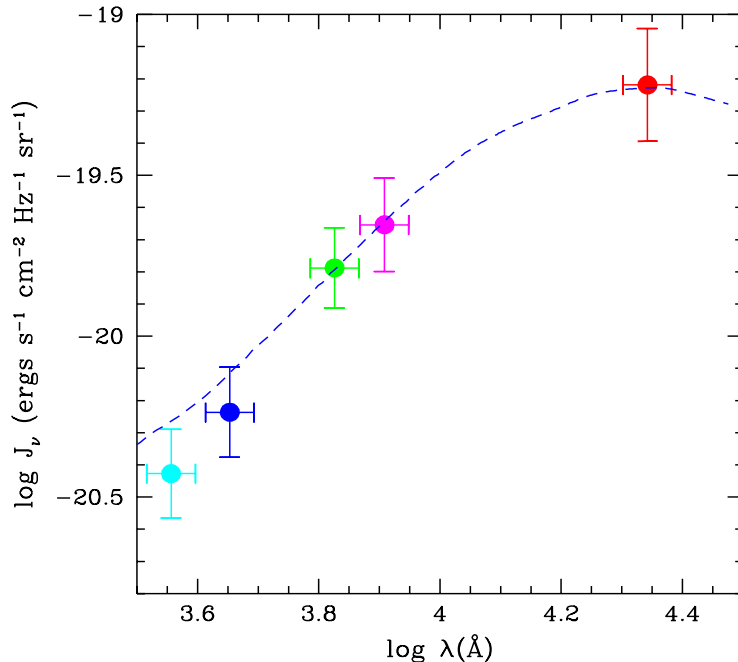


Figure 5. Spectrum of the extragalactic background light as derived from a compilation of ground-based and HDF galaxy counts (see Pozzetti et al. 1997). The 2σ error bars arise mostly from field-to-field variations. *Dashed line*: Model predictions for the fiducial model (star formation history of Figure 3).

5. Clues to Galaxy Formation and Evolution

The results shown in the previous section have significant implications for our understanding of the global history of star and structure formation. Here I discuss a few key issues which will assist in interpreting the evolution of luminous matter in the universe.

5.1. The Brightness of the Night Sky

An important check on the inferred emission history of field galaxies comes from a study of the extragalactic background light (EBL), an indicator of the total optical luminosity of the universe. The contribution of known galaxies to the EBL can be calculated directly by integrating the emitted flux times the differential galaxy number counts down to the detection threshold. I have used a compilation of ground-based and HDF data down to very faint magnitudes (Pozzetti et al. 1997; Williams et al. 1996) to compute the mean surface brightness of the night sky between 0.35 and 2.2 μm . The results are plotted in Figure 5, along with the EBL spectrum predicted by our modeling of the galaxy luminosity density,

$$J_\nu = \frac{1}{4\pi} \int_0^\infty dz \frac{dl}{dz} \rho_\nu(z) \quad (8)$$

where $\nu' = \nu(1+z)$ and dl/dz is the cosmological line element. The overall agreement is remarkably good, with the model spectrum being only slightly bluer, by about 20–30%, than the observed EBL. The straightforward conclusion of this exercise is that *the star formation history depicted in Figure 3 appears able to account for the entire background light recorded in the galaxy counts down to the very faint magnitudes probed by the HDF.*

5.2. Luminous Mass-To-Light Ratios of Present-Day Galaxies

The fiducial Salpeter IMF model generates a present-day stellar mass density of $\Omega_s h_{50}^2 \approx 0.004$, about 10% of the nucleosynthesis constrained baryon density, $\Omega_b h_{50}^2 \approx 0.05 \pm 0.01$ (Walker et al. 1991). The (luminosity-weighted) visible mass-to-light ratios range from about 4 in the B -band to 1 in K , consistent with the values observed in nearby galaxies of various morphological types (see, e.g., Persic & Salucci 1992 and references therein). Note, however, that the predicted M/L are quite sensitive to the lower-mass cutoff of the IMF, as very-low mass stars can contribute significantly to the mass but not to the integrated light of the whole stellar population. For example, a lower cutoff of $0.2 M_\odot$ instead of the $0.1 M_\odot$ adopted would decrease the mass-to-light ratio by a factor of 1.3. Although one could in principle reduce the inferred star formation density by adopting a top-heavy IMF, richer in massive UV-producing stars, in practice a significant amount of dust reddening – hence of “hidden” star formation – would then be required to match the observed galaxy colors. The net effect of this operation would be a baryonic mass comparable to the estimate above and a large infrared background.

5.3. Evolution of the Supernova Rate with Redshift

In recent years there has been a renewed interest in the search for supernovae. While SN Ia may provide one of the best distance indicators at high redshifts (Kim et al. 1997), a direct measurement of the rate of Type II SNe could be used as an independent test for the star formation and heavy element enrichment history of the universe. Figure 6 shows the normalized rate of core-collapse SNe predicted by our best-fit model as a function of cosmic time. The frequency is computed in the rest-frame of the supernovae, and is expressed in SNu (SNe per $10^{10} L_\odot(B)$ per century). Unlike the rate per unit comoving volume, which will trace the rise, peak, and drop of the star formation density, the blue luminosity-weighted frequency is a monotonic increasing function of redshift. The predicted rate is in good agreement (to within 0.2 in the log) with the local values estimated by van den Bergh & Tammann (1991), and Cappellaro et al. (1997). In the near future, ongoing searches for distant SNe should provide enough data to constrain the star formation history of the universe at intermediate redshifts, $z \approx 0.5 - 1$ (Della Valle & Madau 1997).

5.4. Star Formation at High Redshifts: Monolithic Collapse Versus Hierarchical Clustering Models

The biggest uncertainty present in our estimates of the star formation density at $z > 2$ is probably associated with dust reddening, but, as the color-selected HDF sample includes only the most actively star-forming young objects, one could also imagine the existence of a large population of relatively old or faint galaxies still undetected at high- z . The issue of the amount of star formation at early epochs is a non trivial one, as the two competing models, monolithic collapse versus hierarchical clustering, make very different predictions in this regard. From stellar population studies we know in fact that about half of the present-day stars are contained in spheroidal systems, i.e., elliptical galaxies and spiral galaxy bulges (Schechter & Dressler 1987). In the monolithic scenario these formed early and rapidly, experiencing a bright starburst phase at high- z (Eggen, Lynden-Bell, & Sandage 1962; Tinsley & Gunn 1976). In hierarchical clustering theory instead

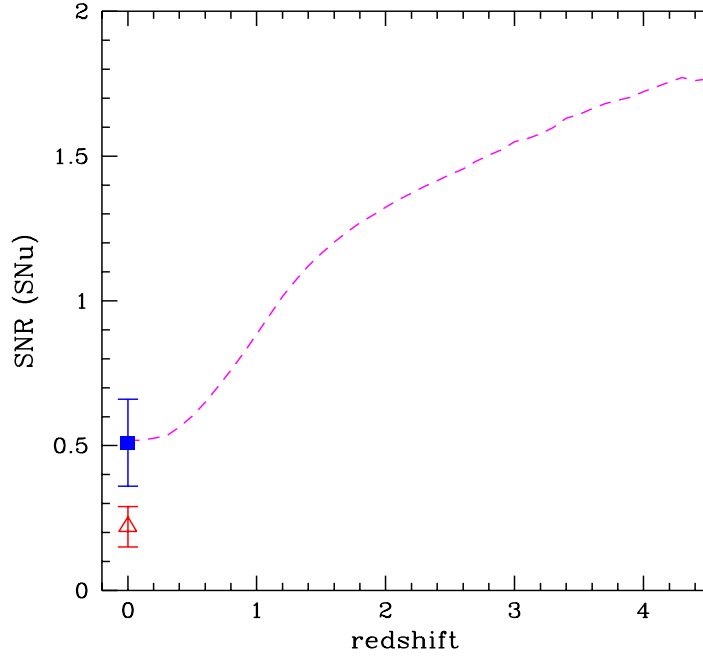


Figure 6. Rest-frame rate of core-collapse supernovae (Type II+Ib/c) in SNU (SNe per $10^{10} L_{\odot}(B)$ per century) versus redshift. The data points with error bars are taken from van den Bergh & Tammann (1991) (*filled square*), and Cappellaro et al. (1997) (*empty triangle*). They have been normalized according to the local blue luminosity function by spectral type of Heyl et al. (1997). The *dashed line* depicts the rate predicted from our Salpeter IMF, $E(B - V) = 0.1$ fiducial model, assuming a lower mass cutoff for the progenitors of $10 M_{\odot}$.

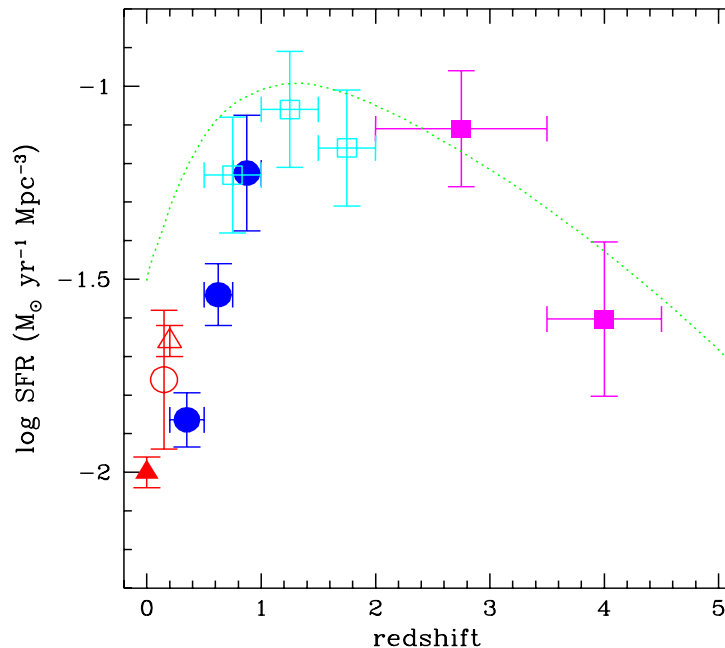


Figure 7. Cosmic star formation history. The data points with error bars are taken from the UV broadband measurements of Lilly et al. (1996) (*filled dots*), Connolly et al. (1997) (*empty squares*), Madau et al. (1996) and Madau (1997) (*filled squares*), Treyer et al. (1997) (*empty dot*). Also plotted are the determinations from the H α luminosity functions of Gallego et al. (1995) (*filled triangle*) and Tresse & Maddox (1997) (*empty triangle*). The data points have been converted to total SFR assuming a Salpeter IMF and a universal $E(B - V) = 0.1$. Because of dust extinction, the observed rest-frame UV fluxes have been corrected upwards by a factor of 1.4 at 2800 Å and 2.1 at 1500 Å. The *dotted line* depicts the SFR per comoving volume predicted by a fiducial CDM model in which structure forms hierarchically (from Cole et al. 1994).

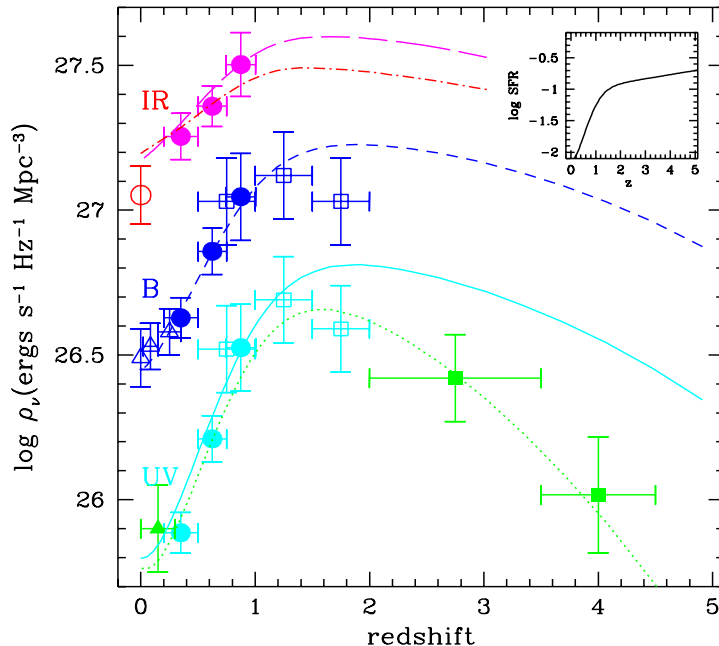


Figure 8. Test case with a much larger star formation density at high redshift than indicated by the HDF dropout analysis. The model – designed to mimick a “monolithic collapse” scenario – assumes a Salpeter IMF and a dust opacity which increases rapidly with redshift, $E(B - V) = 0.011(1 + z)^{2.2}$. Notation is the same as in Figure 3.

ellipticals form continuously by the merger of disk/bulge systems (Kauffman et al. 1993), and most galaxies never experience star formation rates in excess of a few solar masses per year (Baugh et al. 1997). Figure 7 shows the star formation history predicted by a fiducial CDM model (normalized to reproduce the abundance of rich clusters, Cole et al. 1994) and compared to observational estimates. Overall, the agreement between theoretical predictions and data is quite good. Both appear to produce only a small fraction, about 15 – 20%, of the current stellar content of galaxies at $z \gtrsim 2 - 2.5$. In fact, the tendency to form the bulk of the stars at relatively low redshifts is a generic feature not only of the $\Omega_0 = 1$ CDM cosmology, but also of successful low-density CDM models (Cole et al. 1994; Baugh et al. 1997). While uncertainties still remain in this comparison – e.g., because of the poorly known effects of dust obscuration and possible incompleteness in the high- z sample – one should note the tendency of the theoretical curve to sit above the data points at all epochs, thereby predicting luminosity-weighted mass-to-light ratios at the present time which are higher than observed.

It is of interest then to ask how much larger could the volume-averaged SFR at high- z be before its fossil records – in the form of long-lived, near solar-mass stars – became easily detectable as an excess of K -band light at late epochs. In particular, is it possible to envisage a model where 50% of the present-day stars formed at $z > 2.5$ and were

shrouded by dust? The predicted emission history from such a model is depicted in Figure 8. To minimize the long-wavelength emissivity associated with the radiated ultraviolet light, a Salpeter IMF has been adopted. Consistency with the HDF data has been obtained assuming a dust extinction which increases rapidly with redshift, $E(B-V) = 0.011(1+z)^{2.2}$. This results in a correction to the rate of star formation of a factor ~ 5 at $z = 3$ and ~ 15 at $z = 4$. The total stellar mass density today is $\rho_s(0) = 5.0 \times 10^8 \text{ M}_\odot \text{ Mpc}^{-3}$ ($\Omega_s h_{50}^2 = 0.007$).

Overall, the fit to the data is still acceptable, showing how the blue and near-IR light at $z < 1$ are *relatively poor indicators of the star formation history at early epochs*. The reason for this is the short timescale available at $z \gtrsim 2$, which makes the present-day stellar mass density rather insensitive to a significant boost of the stellar birthrate at high redshifts. By contrast, variations in the global SFR around $z \sim 1.5$, where the bulk of the stellar population was assembled, have a much larger impact. The adopted extinction-redshift relation, in fact, implies negligible reddening at $z \lesssim 1$. Relaxing this – likely unphysical – assumption would cause the model to significantly overproduce the K -band local luminosity density. I have also checked that an even larger amount of hidden star formation at early epochs, as recently advocated by Rowan-Robinson et al. (1997) and Meurer et al. (1997), would generate too much blue, $1 \mu\text{m}$ and $2.2 \mu\text{m}$ light to be still consistent with the observations. An IMF which is less rich in massive stars would only exacerbate the discrepancy.

5.5. The Ultraviolet Colors of Lyman-Break Galaxies

Figure 9 shows a comparison between the HDF data and the model predictions for the evolution of galaxies in the $U - B$ vs. $V - I$ color-color plane according to the star formation history of Figure 3. The HDF ultraviolet passband – which is bluer than the standard ground-based U filter – permits the identification of star-forming galaxies in the interval $2 \lesssim z \lesssim 3.5$. Galaxies in this redshift range predominantly occupy the top left portion of the $U - B$ vs. $V - I$ color-color diagram because of the attenuation by the intergalactic medium and intrinsic absorption (M96). Galaxies at lower redshift can have similar $U - B$ colors, but are typically either old or dusty, and are therefore red in $V - I$ as well.

It is clear that the Salpeter IMF, $E(B - V) = 0.1$ model reproduces quite well the rest-frame UV colors of high- z objects in HDF. This may suggest that interstellar dust is already present in these young galaxies and that it attenuates their 1500 \AA luminosities by a factor of ~ 2 . A UV extinction of about 1 mag is also indicated by a comparison between UV and $H\beta$ luminosities in three bright UV dropouts (Pettini et al. 1997). One should note that the prescription for a “correct” de-reddening of the Lyman-break galaxies at $z \sim 3$ is the subject of an ongoing debate (e.g., Meurer et al. 1997; Dickinson et al. 1997; Pettini et al. 1997). Adopting the greyer extinction law deduced by Calzetti et al. (1994) from the integrated spectra of nearby starbursts would require larger corrections to the SFR at high- z in order to match the observed colors. The consequence of this, however, would be the overproduction of red light at low redshifts, as noted in § 5.4. Redder spectra can also result from an aging population or an IMF which is, at early epochs, less rich in massive stars than the adopted ones.

5.6. Constraints from the Mid- and Far-Infrared Background

Ultimately, it should be possible to set some constraints on the total amount of star formation that is hidden by dust over the entire history of the universe by looking at the cosmic infrared background (CIB) (Fall et al. 1996; Burigana et al. 1997; Guiderdoni et al. 1997). Studies of the CIB provide information which is complementary to that given by optical observations. If most of the star formation activity takes place within dusty

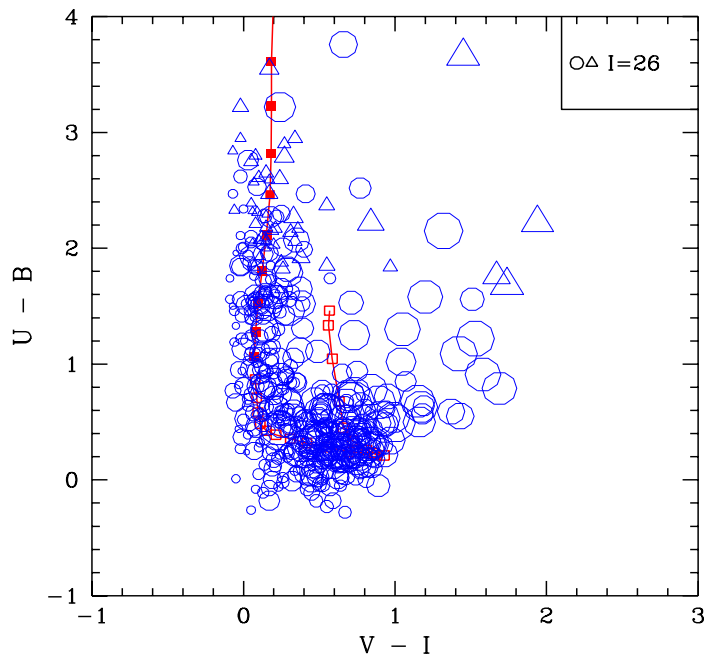


Figure 9. *Solid line*: model predictions for the color evolution of galaxies according to the star formation history of Figure 3. The points (*filled squares* for $z > 2$ and *empty squares* for $z < 2$) are plotted at redshift interval $\Delta z = 0.1$. *Empty circles* and *triangles*: colors of galaxies in the HDF with $22 < B < 27$. Objects undetected in U (with $S/N < 1$) are plotted as triangles at the 1σ lower limits to their $U - B$ colors. Symbols size scales with the I mag of the object, and all magnitudes are given in the AB system. The “plume” of Lyman-break galaxies is clearly seen in the data.

gas clouds, the starlight which is absorbed by various dust components will be reradiated thermally at longer wavelengths according to characteristic IR spectra. The energy in the CIB would then exceed by far the entire background optical light which is recorded in the galaxy counts.

From an analysis of the smoothness of the *COBE* DIRBE maps, Kashlinsky et al. (1996) have recently set an upper limit to the CIB of $10\text{--}15 \text{ nW m}^{-2} \text{ sr}^{-1}$ at $\lambda = 10\text{--}100 \mu\text{m}$ assuming clustered sources which evolve according to typical scenarios. An analysis using data from *COBE* FIRAS by Puget et al. (1996) (see also Fixsen et al. 1996) has revealed an isotropic residual at a level of $3.4 (\lambda/400\mu\text{m})^{-3} \text{ nW m}^{-2} \text{ sr}^{-1}$ in the $400\text{--}1000 \mu\text{m}$ range, which could be the long-searched CIB. The detection, recently revisited by Guiderdoni et al. (1997), should be regarded as uncertain since it depends critically on the subtraction of foreground emission by interstellar dust.

By comparison, the total amount of starlight that is absorbed by dust and reprocessed in the infrared is $7.5 \text{ nW m}^{-2} \text{ sr}^{-1}$ in the model depicted in Figure 3, about 30% of the total radiated flux. The monolithic collapse scenario of Figure 8 generates $6.5 \text{ nW m}^{-2} \text{ sr}^{-1}$ instead. The resulting CIB spectrum is expected to be rather flat because of the spread in the dust temperatures – cool dust will likely dominate the long wavelength emission, warm small grains will radiate mostly at shorter wavelengths – and the distribution in redshift. While both models appear then to be consistent with the data (given the large uncertainties associated with the removal of foreground emission and with the observed and predicted spectral shape of the CIB), it is clear that too much infrared light would be generated by scenarios that have significantly larger amount of hidden star formation at early and late epochs.

5.7. Chemical Enrichment

We may at this stage use our set of models to establish a cosmic timetable for the production of heavy elements (with atomic number $Z \geq 6$) in relatively bright field galaxies (see M96). What we are interested in here is the universal rate of ejection of newly synthesized material. In the approximation of instantaneous recycling, the metal ejection rate per unit comoving volume can be written as

$$\dot{\rho}_Z = y(1 - R) \times \text{SFR}, \quad (9)$$

where the *net*, IMF-averaged yield of returned metals is

$$y = \frac{\int m p_{\text{zm}} \phi(m) dm}{(1 - R) \int m \phi(m) dm}, \quad (10)$$

p_{zm} is the stellar yield, i.e., the mass fraction of a star of mass m that is converted to metals and ejected, and the dot denotes differentiation with respect to cosmic time.

The predicted end-products of stellar evolution, particularly from massive stars, are subject to significant uncertainties. These are mainly due to the effects of initial chemical composition, mass-loss history, the mechanisms of supernova explosions, and the critical mass, M_{BH} , above which stars collapse to black holes without ejecting heavy elements into space (Maeder 1992; Woosley and Weaver 1995). The IMF-averaged yield is also very sensitive to the choice of the IMF slope and lower-mass cutoff. For a Scalo IMF in the assumed mass range ($0.1 < M < 125 M_{\odot}$), for example, the net yield is typically a factor of 3.3 lower than Salpeter. At the same time, a lower cutoff of $0.5 M_{\odot}$ would boost the net yield by a factor of 1.9 for Salpeter and 1.7 for Scalo. Note that some of these ambiguities partially cancel out when computing the total metal ejection rate, as the product $y \times \text{SFR}$ is less sensitive to the slope of the IMF than the yield or the rate of star formation, and is insensitive to the lower mass cutoff. Observationally, the best-fit “effective yield” (derived assuming a closed box model) is $0.025 Z_{\odot}$ for Galactic halo clusters, $0.3 Z_{\odot}$ for disk clusters,

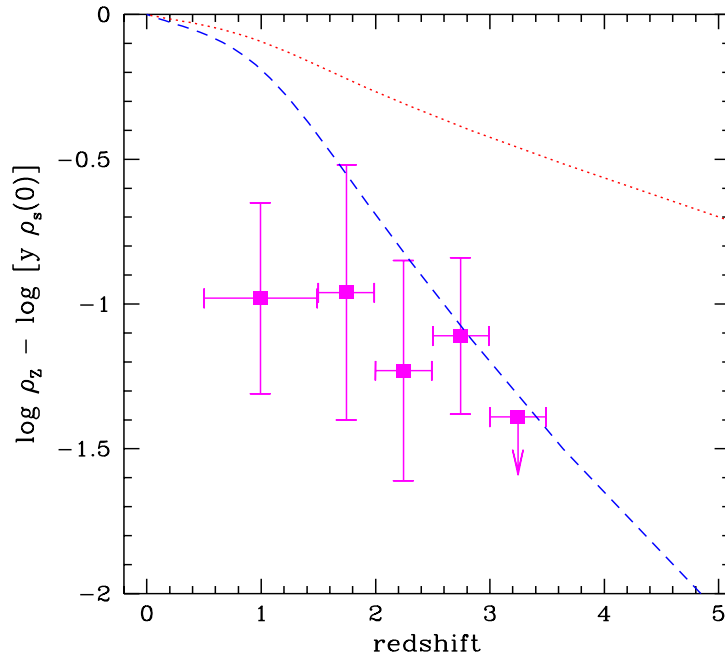


Figure 10. Total mass of heavy elements ever ejected versus redshift for the Salpeter IMF model of Figure 3 (*dashed line*) and the monolithic collapse model of Figure 8 (*dotted line*), normalized to $y\rho_s(0)$, the total mass density of metals at the present epoch. *Filled squares*: column density-weighted metallicities (in units of solar) as derived from observations of the damped Lyman- α systems (Pettini et al. 1997).

$0.4Z_\odot$ for the solar neighborhood, and $1.8Z_\odot$ for the Galactic bulge (Pagel 1987). The last value may represent the universal true yield, while the lower effective yields found in the other cases may be due, e.g., to the loss of enriched material in galactic winds.

Figure 10 shows the total mass of metals ever ejected, ρ_Z , versus redshift, i.e., the sum of the heavy elements stored in stars and in the gas phase as given by the integral of equation (9) over cosmic time. The values plotted have been computed from the star formation histories depicted in Figures 3 and 8, and have been normalized to $y\rho_s(0)$, the mass density of metals at the present epoch according to each model. A characteristic feature of the two competing scenarios is the rather different average metallicity expected at high redshift. For comparison, I have also plotted the *gas metallicity*, Z_{DLA}/Z_\odot , as deduced from observations by Pettini et al. (1997) of the damped Lyman- α systems (DLAs). At early epochs, when the gas consumption into stars is still low, the metal mass density predicted from these models gives, in a closed box model, a measurement of the metallicity of the gas phase. If DLAs and star-forming field galaxies have the same level of heavy element enrichment, then one would expect a rough agreement between Z_{DLA} and the model predictions at $z \gtrsim 3$. This is not true at $z \lesssim 2$, when a significant fraction of heavy

elements is locked into stars.³ From Figure 10, it does appear that the monolithic collapse model overpredicts the cosmic metallicity at high redshifts as sampled by the DLAs. In order for such a model to be acceptable, the gas traced by the DLAs would have to be physically distinct from the luminous star formation regions observed in the Lyman-break galaxies, and to be substantially under-enriched in metals compared to the cosmic mean.

5.8. The Cluster-Field Analogy

It has been recently pointed out by Renzini (1997) and Mushotzky & Loewenstein (1997) that, in the absence of any systematic cluster/field differences, clusters of galaxies may also provide an indication of the metal formation history of the universe. In the fiducial model of Figure 3, the global mean metallicity of the local universe is $y\Omega_s/\Omega_b \sim 0.1y/Z_\odot$ solar, to be compared with the overall cluster metal abundance, $\sim 1/3$ solar. If $y \sim Z_\odot$, the efficiency of metal production must have been larger in clusters than in the field, in spite of both having a similar baryon-to-star conversion efficiency, $\Omega_s/\Omega_b \sim 10\%$. Cluster-related processes, like ram-pressure stripping, would then be responsible for enriching the intracluster medium. Alternatively, a larger IMF-averaged metal yield, $y \sim 3Z_\odot$, may solve the apparent discrepancy. In this case, field galaxies would have to have ejected most of the heavy elements they produce, and there should be a comparable share of metals in the intergalactic medium (IGM) as there is in the intracluster gas. The characteristic metal ejection rate per unit comoving volume associated with such a pollution level would be large,

$$\dot{\rho}_{Z,IGM} \approx (0.013 M_\odot \text{ yr}^{-1} \text{ Mpc}^{-3}) \left(\frac{\Omega_{IGM} h_{50}^2}{0.05} \right) \left(\frac{3Z_{IGM}}{Z_\odot} \right) \left(\frac{f_{inj}}{0.7} \right)^{-1} \left(\frac{\Delta t}{2.5 \text{ Gyr}} \right)^{-1}, \quad (11)$$

about ten times larger than derived at $z = 2$ from our modeling of the galaxy emission history (with $y \sim Z_\odot$). Here, Ω_{IGM} is the baryonic density parameter of the IGM phase and f_{inj} is the fraction of heavy elements injected into the IGM during a timescale Δt . It is hard to see, however, how massive galaxies with deep potential wells could be responsible for large outflows of metal-enriched gas. Recent observations of metal lines in the Ly α forest clouds at $z \sim 3$, while pointing towards some widespread chemical enrichment at early epochs, suggest typical metallicities of only 0.003 to 0.01 solar (Cowie et al. 1995). Similar low values have been inferred in local Ly α absorbers (Shull et al. 1997).

Acknowledgments. It is a pleasure to thank the hospitality of the European Southern Observatory, Garching, where this review was largely written. I have benefited from many useful discussions on various topics related to this talk with C. Baugh, G. Bruzual, S. Charlot, A. Connolly, M. Della Valle, M. Pettini, A. Renzini, M. Treyer, and my collaborators, L. Pozzetti and M. Dickinson. Support for this work was provided by NASA through grant AR-06337.10-94A from the Space Telescope Science Institute, which is operated by the Association of Universities for Research in Astronomy, Inc., under NASA contract NAS5-26555.

References

- Baugh, C. M., Cole, S., Frenk, C. S., & Lacey, C. G. 1997, ApJ, submitted
 Bower, R. G., Lucey, J. R., & Ellis, R. S. 1992, MNRAS, 254, 589

³More complex chemical evolution models which reproduce the evolving gas content and the metal enrichment history of the DLAs have been developed by Lanzetta, Wolfe, & Turnshek (1995) and Pei & Fall (1995).

- Bruzual, A. G., & Charlot, S. 1993, *ApJ*, 405, 538
- Bruzual, A. G., & Charlot, S. 1997, in preparation
- Bruzual A. G., & Kron, R. G. 1980, *ApJ*, 241, 25
- Burigana, C., Danese, L., De Zotti, G., Franceschini, A., Mazzei, P., & Toffolatti, L. 1997, *MNRAS*, 287, L17
- Calzetti, D., Kinney, A. L., & Storchi-Bergmann, T. 1994, *ApJ*, 429, 582
- Cappellaro, E., Turatto, M., Tsvetkov, D. Yu., Bartunov, O. S., Pollas, C., Evans, R., & Hamuy, M. 1997, *A&A*, 322, 431
- Charlot, S. 1996a, in *From Stars to Galaxies*, ed. C. Leitherer & U. Fritze-von Alvensleben (ASP Conference Series), in press
- Charlot, S. 1996b, in *The Universe at High-z, Large Scale Structure, and the Cosmic Microwave Background*, ed. E. Martinez-Gonzalez & J. L. Sanz (Heidelberg: Springer), p. 53
- Cole, S., Aragón-Salamanca, A., Frenk, C. S., Navarro, J. F., & Zepf, S. E. 1994, *MNRAS*, 271, 781
- Connolly, A. J., Szalay, A. S., Dickinson, M. E., SubbaRao, M. U., & Brunner, R. J. 1997, *ApJ*, in press
- Cowie, L. L., Songaila, A., Hu, E. M., & Cohen, J. G. 1996, *AJ*, 112, 839
- Cowie, L. L., Songaila, A., Kim, T.-S., & Hu, E. M. 1995, *AJ*, 109, 1522
- Della Valle, M., & Madau, P. 1997, in preparation
- Dickinson, M. E. 1997, private communication
- Dickinson, M. E., et al. 1997, in preparation
- Eggen, O. J., Lynden-Bell, D., & Sandage, A. R. 1962, *ApJ*, 136, 748
- Ellis, R. S., Colless, M., Broadhurst, T., Heyl, J., & Glazebrook, K. 1996, *MNRAS*, 280, 235
- Fall, S. M., Charlot, S., & Pei, Y. C. 1996, *ApJ*, 464, L43
- Ferguson, H. C., & Babul, A. 1997, *MNRAS*, in press
- Fixsen, D. J., Cheng, E. S., Gales, J. M., Mather, J. C., Shafer, R. A., Wright, E. L. 1996, *ApJ*, 473, 576
- Gallego, J., Zamorano, J., Aragón-Salamanca, A., & Rego, M. 1995, *ApJ*, 455, L1
- Gardner, J. P., Sharples, R. M., Frenk, C. S., & Carrasco, B. E. 1997, *ApJ*, 480, L99
- Guiderdoni, B., Bouchet, F. R., Puget, J.-L., Lagache, G., & Hivon, E. 1997, *Nature*, in press
- Heyl, J., Colless, M., Ellis, R. S., & Broadhurst, T. 1997, *MNRAS*, 285, 613
- Kashlinsky, A., Mather, J. C., & Odenwald, S. 1996, *ApJ*, 473, L9
- Kauffmann, G., White, S. D. M., & Guiderdoni, B. 1993, *MNRAS*, 264, 201
- Kennicutt, R. C. 1983, *ApJ*, 272, 54
- Kim, A. G., et al. 1997, *ApJ*, 476, L63
- Koo, D. C. 1985, *AJ*, 90, 418
- Lanzetta, K. M., Wolfe, A. M., & Turnshek, D. A., *ApJ*, 440, 435
- Lilly, S. J., Le Fèvre, O., Hammer, F., & Crampton, D. 1996, *ApJ*, 460, L1
- Lilly, S. J., Tresse, L., Hammer, F., Crampton, D., & Le Fèvre, O. 1995, *ApJ*, 455, 108
- Madau, P. 1995, *ApJ*, 441, 18
- Madau, P. 1997, in *Star Formation Near and Far*, ed. S. S. Holt & G. L. Mundy, (AIP: New York), p. 481

- Madau, P., Ferguson, H. C., Dickinson, M. E., Giavalisco, M., Steidel, C. C., & Fruchter, A. 1996, *MNRAS*, 283, 1388 (M96)
- Madau, P., Pozzetti, L., & Dickinson, M. E. 1997, *ApJ*, in press
- Maeder, A. 1992, *A&A*, 264, 105
- Meurer, G. R., Heckman, T. M., Lehnert, M. D., Leitherer, C., & Lowenthal, J. 1997, *AJ*, 114, 54
- Mushotzky, R. F., & Loewenstein, M. 1997, *ApJ*, 481, L63
- Ortolani, S., Renzini, A., Gilmozzi, R., Marconi, G., Barbuy, B., Bica, E., & Rich, M. R. 1995, *Nature*, 377, 701
- Pagel, B. E. J. 1987, in *The Galaxy*, ed. G. Gilmore & B. Carswell (Dordrecht: Reidel), p. 341
- Pei, Y. C. 1992, *ApJ*, 395, 130
- Pei, Y. C., & Fall, S. M. 1995, *ApJ*, 454, 69
- Persic, M., & Salucci, P. 1992, *MNRAS*, 258, 14P
- Pettini, M., Smith, L. J., King, D. L., & Hunstead, R. W. 1997, *ApJ*, in press
- Pettini, M., Steidel, C. C., Dickinson, M., Kellogg, M., Giavalisco, M., & Adelberger, K. L. 1997, in *The Ultraviolet Universe at Low and High Redshift*, ed. W. Waller, (Woodbury: AIP Press), in press
- Pozzetti, L., Bruzual, G. A., & Zamorani, G. 1996, *MNRAS*, 281, 953
- Pozzetti, L., Madau, P., Zamorani, G., Ferguson, H. C., & Bruzual, G. A. 1997, *MNRAS*, submitted
- Puget, J.-L., Abergel, A., Bernard, J.-P., Boulanger, F., Burton, W. B., Desert, F.-X., & Hartmann, D. 1996, *A&A*, 308, L5
- Renzini, A. 1997, *ApJ*, in press
- Rowan-Robinson, M., et al. , 1997, *MNRAS* 289, 490
- Ruiz-Lapuente, P., Canal, R., & Burkert, A. 1997, in *Thermonuclear Supernovae*, ed. P. Ruiz-Lapuente, R. Canal, & J. Isern (Dordrecht: Kluwer), in press
- Salpeter, E. E. 1955, *ApJ*, 121, 161
- Saunders, W., Rowan-Robinson, M., Lawrence, A., Efstathiou, G., Kaiser, N., Ellis, R. S., & Frenk, C. S. 1990, *MNRAS*, 242, 318
- Scalo, J. N. 1986, *Fundam. Cosmic Phys.*, 11, 1
- Schechter, P. L., & Dressler, A. 1987, *AJ*, 94, 56
- Shull, J. M., Penton, S., Stocke, J. T., Giroux, M. L., van Gorkom, J. H., & Carilli, C. 1997, in preparation
- Soifer, B. T., & Neugebauer, G. 1991, *AJ*, 101, 354
- Tinsley, B. M. 1980, *Fundam. Cosmic Phys.*, 5, 287
- Tinsley, B. M., & Gunn, J. E. 1976, *ApJ*, 203, 52
- Tresse, L., & Maddox, S. J. 1997, preprint
- Treyer, M. A., Ellis, R. S., Milliard, B., & Donas, J. 1997, in *The Ultraviolet Universe at Low and High Redshift*, ed. W. Waller, (Woodbury: AIP Press), in press
- van den Bergh, S., & Tammann, G. A. 1991, *ARA&A*, 29, 363
- Walker, T. P., Steigman, G., Schramm, D. N., Olive, K. A., & Kang, H. 1991, *ApJ*, 376, 51
- White, S. D. M., & Frenk, C. S. 1991, *ApJ*, 379, 25
- Williams, R. E., et al. 1996, *AJ*, 112, 1335

Woosley, S. E., & Weaver, T. A. 1995, ApJS, 101, 181
Yungelson, L., & Livio, M. 1997, ApJ, submitted